Supporting Information

Unravelling the last milliseconds of an individual graphene nanoplatelet before impact with a Pt surface by bipolar electrochemistry

Zejun Deng[1,†], *and Christophe Renault*[1,*]

[1] Laboratoire de Physique de la Matière Condensée, Ecole Polytechnique, CNRS, IP Paris, Route de Saclay, 91128, Palaiseau, France

[†] Present address: Institute for Health Innovation & Technology, National University of Singapore, Singapore 117599, Singapore

*Corresponding author, E-mail address: christophe.reanult@polytechnique.edu

---

Table of Contents

1. Chemicals and materials

The 4 mM 1,1'-ferrocendimethanol (FcDM) solution is prepared by dissolving FcDM powder (Sigma) in 0.01% v/v poly(4-styrene sulfonic acid) (PSS) aqueous solution. We observed that PSS increases the solubility of FcDM (usually limited to 2 mM in water). The solution was sonicated for 15 min and then filter with a 0.2 µm syringe filter. The solution was stocked in the fridge (4 °C) when not used and the aliquots used for experiments were discarded at the end of the day. A new solution was prepared every week.

The concentration of GNP and FcDM in the solution used for the opto-electrochemical measurements was measured by UV-Visible absorption (Cary 50 Scan, Variant). First, we prepared suspensions of GNP at different known concentrations (9, 4.5, 2.25, 0.9 mg/mL in 0.01% v/v PSS aqueous solution) and measured a spectrum right after sonication. Based on these spectra we determined the extinction coefficient of GNP (Figure S1 A). We determined, in the same manner, the extinction coefficient of FcDM (Figure S1 B). The continuous absorption of GNP in the visible range leads to a black color while the absorption peak of FcDM at 432 nm gives a yellow color. The blank of the cuvette with 0.01% v/v PSS aqueous solution is systematically subtracted. The concentration of GNP and FcDM was determined using the extinction spectrum of each species and Beer-lambert law:

$$A = \varepsilon l c$$

with the length of the optical cuvette, l, being fixed (l =1 cm) and the concentration, C, of the species. The concentration of FcDM is 3.5 mM while the concentration of GNP in the opto-electrochemical cell is 0.43 mg/mL. This mass concentration can be converted in molar concentration assuming that GNPs are 4.2 µm diameter and 15 nm thick disks and using the equation:

$$C_{(mol.L^{-1})} = C_{(g.L^{-1})} \frac{1}{N_A \rho V_{GNP}}$$

where N_A, ρ and V_{GNP} are the Avogadro's constant, the density of HOPG and the average volume of a GNP, respectively. A concentration of 0.43 mg/mL is equivalent to 1.5 pM of "disk-shaped" GNP.

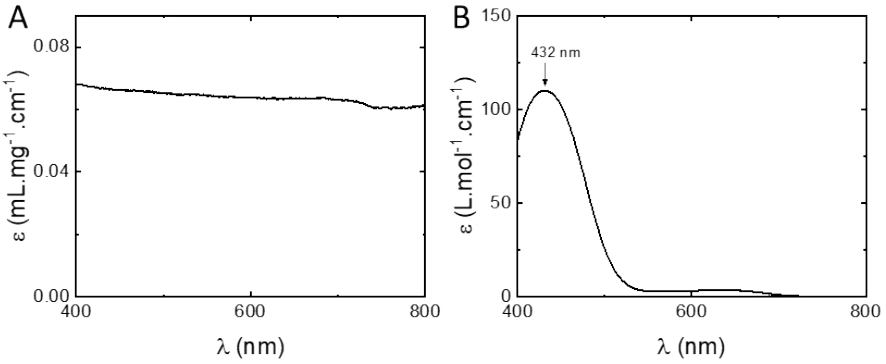

Figure S1. UV-Visible extinction spectra of the GNP (A) and FcDM (B). The optical path is 1 cm.

2. Electrode fabrication

The working electrode is a heat-sealed 10 µm Pt disk electrode. The procedure for the fabrication of the electrode is explained in detail in the following reference.[1] Briefly, a 10 µm Pt wire (Goodfellow, hard temper) is sealed in a borosilicate glass capillary by slowly softening the glass with a heating coil under vacuum. The side of the wire is exposed by polishing the capillary with sandpaper and then alumina slurry (down to 0.1 µm, Buehler) until obtaining a mirror-like surface. The ultra-microelectrode (UME) is sharpened by manually polishing the side of the capillary on sandpaper until achieving an RG = 15 as shown in Figure S2 A (RG is the ratio of the diameter of the glass sheath divided by the diameter of the Pt disk). This step is important not to hinder too much the mass transfer of the GNP from the bulk toward the Pt surface once this later is positioned at 300 µm from the coverslip. Before each experiment, the UME is cleaned by immersion in fresh Piranha for few tens of seconds and rinsed with DI-water. Once a GNP is adsorbed on the UME this latter is systematically cleaned with Piranha before recording a new chronoamperogram.

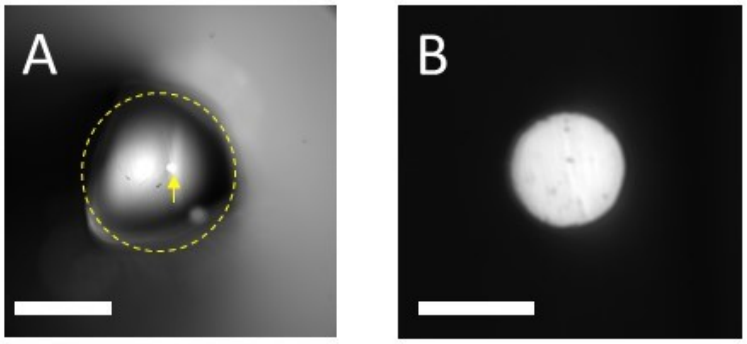

Figure S2. Optical micrographs of the Pt UME taken with a 20X (A) and 100X (B) objective. The scale bars represent 100 µm in (A) and 10 µm in (B). The yellow dashed line represents the edge of the glass sheath surrounding the Pt disk indicated by the arrow.

3. SEM characterization of GNPs

The size and shape of the GNPs were measured by SEM (Hitachi S-4800). A drop of GNPs suspension was incubated for 10 min on a Si wafer (cleaned with Piranha, incubated in a PAA solution and rinsed with DI water) and then gently rinsed with DI water. Typical SEM images are shown in Figure S3A. The ill-defined shape of the GNP does not allow to provide one number to quantify the size of the GNP. We measured the longest and shortest axis of the GNPs and plotted their histogram in Figure S3 B and C respectively. The average longest and shortest axis measure 3.2 ± 2.0 µm and 1.8 ± 1.1 µm, respectively. The in-plane aspect ratio of the GNP is 1.8.

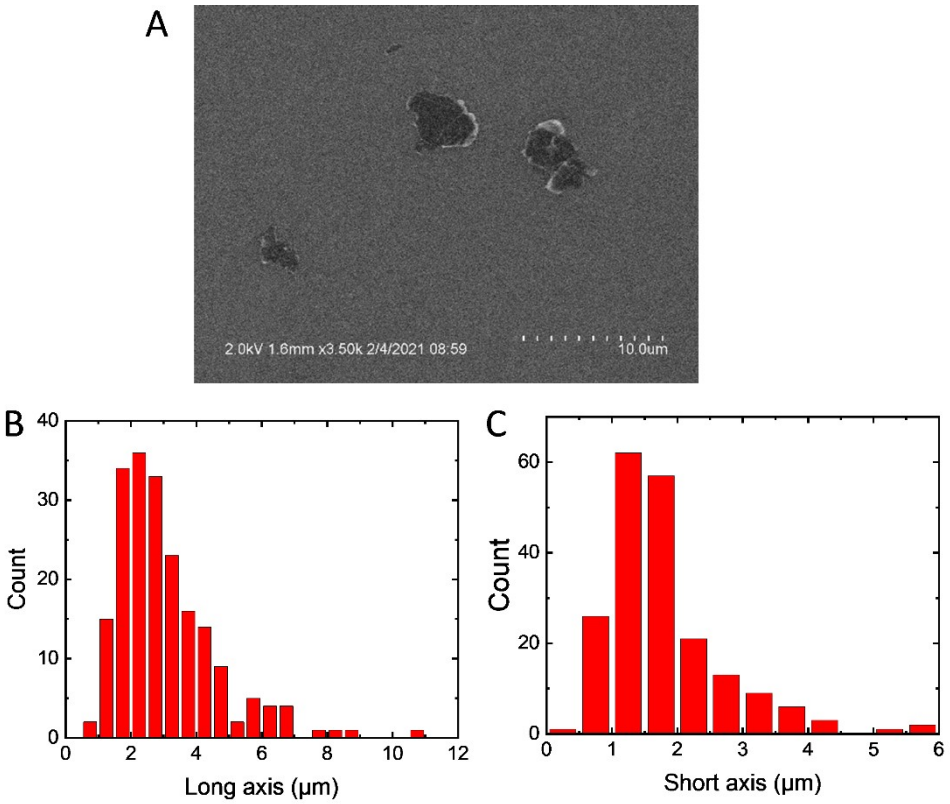

Figure S3. (A) Typical SEM image of GNPs adsorbed on a Si wafer. Histograms of the long (B) and short (C) axis of the GNP measured by SEM over 203 platelets.

4. Image Analysis

A stack of 16-bit unsigned images is recorded for each video. The video is trimmed and then images are cropped in 85 x 85 pixel frames centered around the Pt disk. The color scale is then inverted and the background image (that is before the arrival of the GNP) is subtracted. The background image is constructed by averaging the first 700 frames (in absence of GNP). The difference highlights the difference in reflected light caused by the presence of the GNP. A typical frame before (left) and after processing (right) is shown in Figure S4.

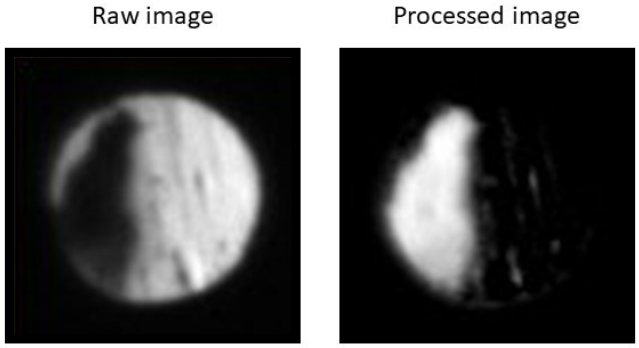

Figure S4. Example of an image acquired during a collision experiment before (left) and after (right) inverting the greyscale and subtracting the background

5. Opto-electrochemical setup

The opto-electrochemical setup is composed of an inverted microscope (ix73, Olympus) and a Faraday cage mounted on the stage of the microscope as shown in the picture in Figure S5 A. A homemade opto-electrochemical cell (see Figure S5 B) allows monitoring the surface of a Pt UME through a 170 ± 5 µm thick coverslip (25 mm diameter n°1.5H, Thorlabs). The cell and the o-ring are made of Teflon and PTFE, respectively. The entire cell is Piranha cleaned between experiments. A leakless Ag/AgCl 3.4 M (Innovative Instruments, Inc) is inserted via a hole on the side of the cell. The UME is positioned at 300 µm from the top side of the coverslip by focusing first on the surface of the coverslip, moving up the objective by 300 µm and then moving the UME down until getting a sharp image. The procedure is performed with a 10X objective and then repeated with a 40X objective in order to have a precision of at least 2 µm (see the calculation of the depth of field at the end of the section). The 10X (UPlanFLN, Olympus) and 40X (LUPlanFLN, Olympus) objectives have a numerical aperture of 0.3 and 0.6, respectively.

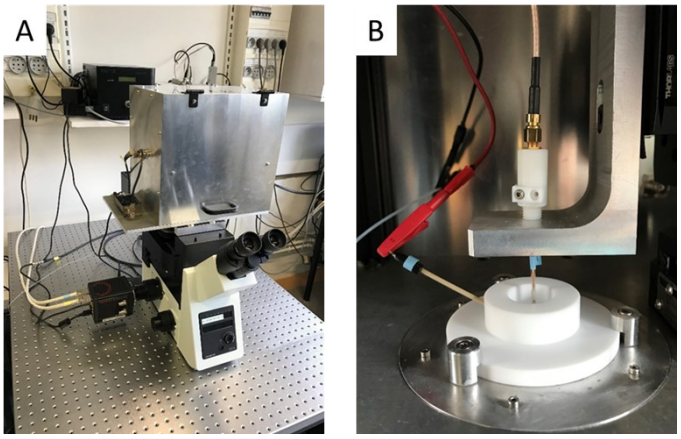

Figure S5. Photographs of the inverted microscope equipped with a Faraday cage (A) and the opto-electrochemical cell (B).

The light source is halogen light (TH4-200, Olympus). The image is collected by a sCMOS camera (OrcaFlash v4 C13440, Hamamatsu). 256 x 256 pixel images are collected with a 16-bit resolution. The software is set to acquire a video at 1kHz and the camera is triggered by an external TTL. The potential applied between the UME and the reference electrode is set by an acquisition card (BNC 2110, National Instrument) using an analog voltage output (a follower amplifier plugged after the card protects this latter from short-circuits) and the current is measured using a trans-impedance amplifier (2V/nA fixed gain, BW 2kHz, LCA-2k-2G, Femto). The output voltage of the amplifier is measured at 2kHz using an analog input of the acquisition card. These operations are triggered by an external trigger (+5V TTL) generated by the card at the beginning of the experiment. The external trigger signal is also sent to the camera via a coaxial cable. An in-house Labview code is used to command the acquisition card. Before each collision measurement, the cleanliness of the electrode is checked optically and electrochemically. We verified (results not shown) that the illumination of the UME does not affect the electrochemical response.

The cell contains typically 5 mL of solution. After spiking the solution with the stock solution of GNP, a glass pipette is used to gently stir the solution and homogenize this latter without forming bubbles. The Faraday cage and the acquisition card are grounded together and connected to the earth. The microscope is placed on top of a floating table (CleanBench, TMC) to reduce mechanical vibrations.

The depth of field of the objectives, *DOF*, is calculated using the relation:[2]

$$DOF = \frac{\lambda n}{NA^2} + \frac{ne}{M \times NA}$$

where λ, n, NA, e and M are the wavelength of the light used for illumination, the index of refraction of the medium between the sample and the objective, the numerical aperture of the objective, the pixel size of the camera and the magnification, respectively. Here, we consider λ = 550 nm (yellow-green), n = 1.3 (average refractive index weighed by the beam path in water (300 µm), glass (170 µm) and air (3000 µm)) and e = 6.5 µm for our camera. With the 40X objective the *DOF* = 2 µm.

6. Blank measurement

Figure S6 shows a chronoamperogram recorded in absence of GNP in solution. The current from FcDM oxidation is observed. No transient current is observed.

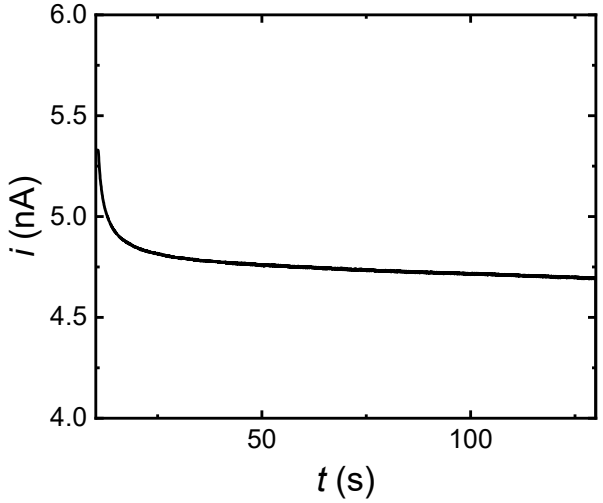

Figure S6. Chronoamperogram recorded in absence of GNP. The solution contains 4 mM of FcDM in 0.01%v/v PSS aqueous solution. The working electrode is a 10 µm diameter Pt UME biased at +0.4 V versus an Ag/AgCl 3.4 M KCl reference electrode.

7. Effect of the viscosity on the velocity of GNP

The effect of the viscosity of solution on the velocity of GNP approaching UME is considered in this section. Figure S7 A, B and C show typical chronoamperograms during the collisions of GNP with a 5 µm radius Pt UME in absence of glycerol (control group), and in presence of 10% v/v and 30% v/v glycerol, respectively. After the addition of glycerol in solution, the diffusion coefficient of FcDM decreases from 6.70 × 10^{-6} cm^2/s (control group) to 4.90 × 10^{-6} cm^2 (10% v/v glycerol) and 2.93 × 10^{-6} cm^2 (30% v/v glycerol) calculated from the steady-state current in respective cyclic voltammograms (not shown). The dynamic viscosity of the mixture of aqueous solution and glycerol can be approximately obtained by the equation:[3]

$$\mu = \mu_{aq}^{\alpha} \mu_{g}^{1-\alpha}$$

Where μ is the dynamic viscosity of the mixture, and subscripts *aq* and *g* denote aqueous solution (here the viscosity is close to 1.0 mPa·s) and the glycerol (1.412 Pa·s), respectively. α is the weighting factor between NaOH solution and glycerol. Then, we obtained the viscosity of the solution of 1.0 mPa·s, 2.1 mPa·s, and 8.8 mPa·s, corresponding to 0, 10 and 30% v/v glycerol, respectively.

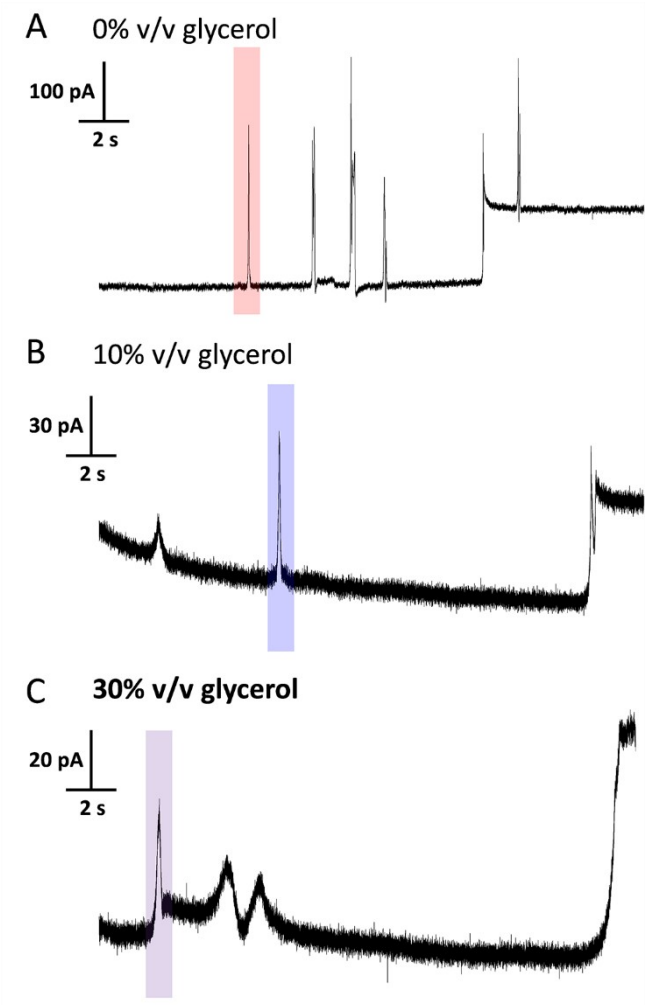

Figure S7. Chronoamperograms recorded at 2 kHz with a 5 µm radius Pt UME at 0.4 V vs Ag/AgCl 3.4 M KCl in presence of (A) 0%, (B) 10% v/v, and (C) 30% v/v glycerol. The enlarged current trace shown in Figure 2 is highlighted in colors, respectively. The solution contains 0.43 mg/ml of GNP, 2 mM FcDM, and 10 µM NaOH. These measurements were done with a pure electrochemical workstation (see our previous reference[4]) in order to obtain the statistical number of collisions within the reasonable experimental time course.

8. Numerical Simulation

The simulations were performed on a PC equipped with 128 GB of RAM and an Intel® Xeon® CPU E5-2699 v4 processor of 2.70 GHz computer with COMSOL 5.3a. The simulations were performed in 2D axial geometry and for steady-state equations. The error arising from using stationary solutions instead of time-dependent solutions was estimated by computing the concentration profile of the stationary (red trace Figure S8) and time-dependent (black trace Figure S8) solution for the simple case of mass transfer limited oxidation at the disk UME with an insulating GNP. The time-dependent solution was computed at a time small enough (0.2 s) so that molecules diffusing from the electrode cannot reach the bulk boundary. The difference between these profiles normalized by the time-dependent solution is plotted in blue in the inset in Figure S8. At the location of the GNP where all the relevant quantities discussed in the present manuscript are computed, the stationary solution underestimates the concentration by less than 8% compared to the time-dependent solution. The error is larger (up to 40%) at 4-5 radius away from the electrode. At these distances, no bipolar feedback can be observed. More importantly, the time-dependent solution is obtained after 238 s while the stationary solution is obtained in only 4 s. For this simple case, the computation of the stationary solution is about 60 times faster than the time-dependent one for only 8% of error. As for the total simulation time for each experiment, the computation of the time-dependent solution takes up to 17901 s while the stationary solution only costs 47 s to compute. Thus, numerical simulations with the stationary solution are considered in this work.

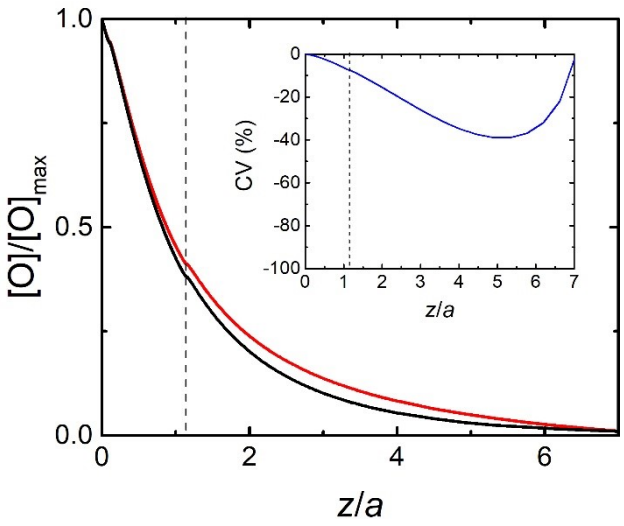

Figure S8. Concentration profiles along the symmetry axis *z* simulated for mass transfer oxidation of 3.4 mM FcDM at an insulating BPE (L = 5 µm, w = 1 µm, d = 0.5 µm) above a disk (a = 5 µm) UME using a steady-state (red trace) and time-dependent (black trace; 0.2 s) diffusion equation. The mesh is similar for both simulations. This inset shows the difference between the stationary and time-dependent profiles divided by the time-dependent profile. The vertical dashed lines indicate the extremity of the GNP in atypical simulation.

Figure S9 represents the domain of 2D axial numerical simulations with the stationary solution. The GNP is a prolate ellipsoid (red line) located above a disk UME (green line). The solution is represented by a quarter of the sphere (blue line).

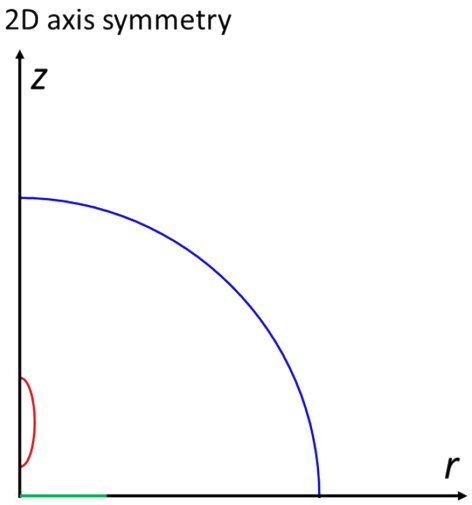

Figure S9. 2D axial geometry used to simulate the electrochemistry of a spheroidal GNP (red line) placed above a disk UME (green line).

The diffusion of the molecules in solution is governed by Fick's law (Transport of Diluted Species module):

$$J = D\nabla C$$

where *J*, *D* and *C* are the flux, diffusion coefficient and concentration of the species, respectively. The potential inside the GNP is governed by Ohm's law (Electric Currents module):

$$\nabla J = 0$$

$$J = \sigma E$$

$$E = -\nabla V$$

where *σ*, *E* and *V* are the conductivity, the electric field and the potential, respectively. The coupling of the two physics occurs at the GNP boundary (same flux condition) where the flux depends on both the concentration of the species and the potential. In order to keep electro-neutrality, we also impose that the net flux of species over the entire surface *S* (i.e. anodic and cathodic sides) equals zero:

$$\int_{\partial\Omega} J dS = 0$$

The flux of the species at the UME and GNP is governed by the Butler-Volmer equation:

$$J = nFDk^{\circ}\left([O]e^{-\frac{\alpha nF}{RT}\left(V - E^{0}\right)} - [R]e^{\frac{(1-\alpha)nF}{RT}\left(V - E^{0}\right)}\right)$$

where *n*, *F*, *k°*, *α*, *R*, *T* and *E°* are the number of electrons exchanged, the Faraday's constant, the standard electron transfer rate constant, the coefficient of symmetry, the gas constant, the temperature and the standard potential of the redox couple, respectively. Note that we use "*V*" to represent the potential of the electrode (UME or GNP). All the boundaries of the simulation are given in Table S1.

Table S1. Boundaries of the simulation.

Color code	Description	Type of boundary*
red line	GNP	$J = nFDk^{\circ}\left([O]_{GNP}e^{-\frac{\alpha nF}{RT}\left(V_{GNP}-E^{0}\right)} - [R]_{GNP}e^{\frac{(1-\alpha)nF}{RT}\left(V_{GNP}-E^{0}\right)}\right)$ and $\int_{\partial\Omega} JdS = 0$
green line	UME	$J = nFDk^{\circ}\left([O]_{UME}e^{-\frac{\alpha nF}{RT}\left(V_{UME}-E^{0}\right)} - [R]_{UME}e^{\frac{(1-\alpha)nF}{RT}\left(V_{UME}-E^{0}\right)}\right)$
blue line	bulk solution	[R] = 3.43 mM; [O] = 0.01[R]
black line	glass sheath and axis of revolution	$\nabla[R] = \nabla[O] = 0$

The total current passing through the GNP is computed using

$$i = sgn\left(\frac{\partial[O]}{\partial r};\frac{\partial[O]}{\partial z}\right)nFD\int\sqrt{\left(\frac{\partial[O]}{\partial r}\right)^2+\left(\frac{\partial[O]}{\partial z}\right)^2}dS \quad \text{for} \quad \frac{\partial[O]}{\partial r} and \frac{\partial[O]}{\partial z} > 0$$

Note that we must integrate only the incoming *or* outgoing flux of O, otherwise the current is doubled. Indeed, at a GNP there is both oxidation and reduction, their current being equal. The current passing through UME is computed using

$$i = nFD\int\sqrt{\left(\frac{\partial[O]}{\partial r}\right)^2+\left(\frac{\partial[O]}{\partial z}\right)^2}dr$$

9. Simulated concentration and potential profiles near UME

Concentration profile near the surface of the UME. Under the condition of electro-neutrality of the GNP, the net current passing through the surface of the GNP must be null (i.e. no charge is being accumulated inside the GNP). The potential inside the GNP is governed by Ohm's law. The diffusion of FcDM and $FcDM^+$ is considerably faster than the motion of GNP observed in the movies (about 1 - 20 µm/s). Consequently, the diffusion profiles of $FcDM^+$ and FcDM "instantaneously" readapt to the position of the GNP and thus we sought for steady-state solutions of the diffusion equation. Figure S10 A shows the simulated concentration map of FcDM in presence of insulating spheroidal particles (i.e. in absence of depolarization by faradaic reaction) near the surface of a UME having their bottom end at 0.5 µm from the surface of the UME. The black lines represent the gradient of concentration (i.e. the flux of species). The gradient of concentration displays a radial symmetry and is the strongest near the surface of the UME quickly decaying after a couple of electrode's radius. The overpotential applied at the UME (E_{WE} - $E°$= 0.4 V) is sufficiently large to reach mass transfer limited currents.

Potential profile near the surface of the UME. The concentration profile near the surface of the UME is described by the Nernst equation:

$$E = E^0 - \frac{RT}{nF} ln\left(\frac{[R]}{[O]}\right)$$

where *E* represents the potential of the electrons in the metal phase at equilibrium with the species O and R in solution, E^0 is the formal potential of the $FcDM^+$/FcDM redox couple, *R* is the gas constant, *T* is the temperature, n is the number of electrons exchanged, *F* is the Faraday's constant. The potential map near the surface of the UME can be obtained by using the concentration profile and Nernst equation, as shown in Figure S10 B.

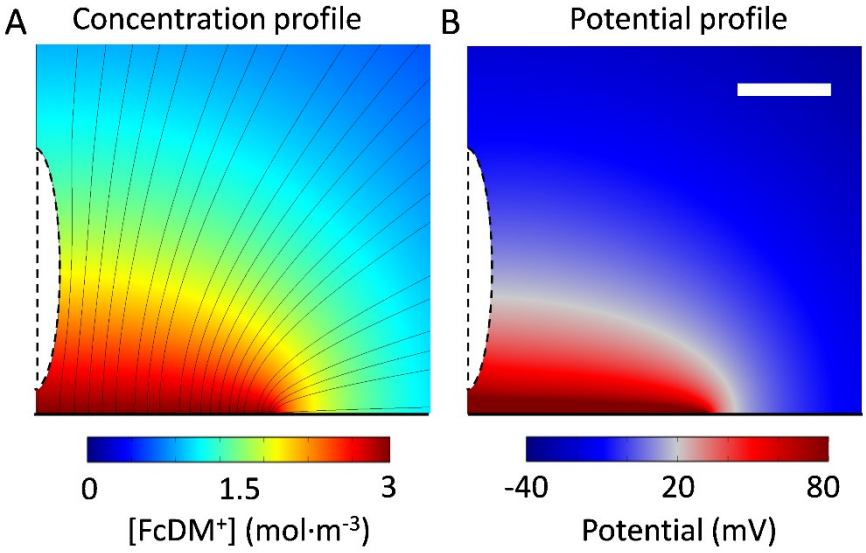

Figure S10. (A) Concentration profile of $FcDM^+$ in presence of an insulating spheroidal particles (5 µm tall and 1 µm wide) near the surface of the UME at a steady state. The black lines represent the normal flux of $FcDM^+$. (B) Potential profile of insulating particles calculated from the concentration profile in (A) via Nernst equation. The scale bar represents 2 µm. The parameters of the simulation are: [FcDM] = 3.431 mM, [$FcDM^+$] = 0.035 mM, E_{WE} = 0.4 V, n = 1, α = 0.5, k^0 = 10 cm·s^{-1}, σ_{GNP} = 6 x 10^6 S·cm^{-1}, D_{FcDM} = D_{FcDM}+ = 6.5 x 10^{-6} cm^2·s^{-1}, a = 5 µm, *L* = 5 µm, *W* = 1 µm, *d* = 0.5 µm, T = 298 K.

10. Effect of the initial ratio [O]/[R] on the bipolar current

Figure S11 shows the simulated bipolar current, i_{BPE}, normalized by the steady-state current at the UME, i_{ss}, as a function of various ratios between oxidized and reduced species, [O]/[R]. Since the steady-state current at the UME is linearly proportional to the concentrations of [R], we normalized the bipolar current by i_{ss} to exclusively study the effect of initial ratio [O]/[R] on the bipolar current. The normalized bipolar current passing through the GNP is constant with the increase of the initial ratio [O]/[R], indicating that the bipolar current is independent of the initial bulk ratio [O]/[R].

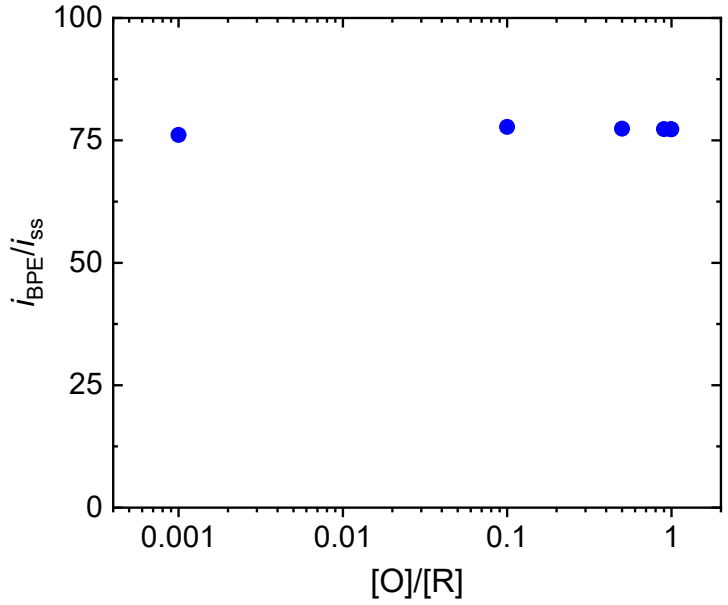

Figure S11. Effect of the initial ratio [O]/[R] on the bipolar current. Each blue point corresponds to the specific ratio of [O]/[R].

11. Collection efficiency

The current in absence of GNP is computed with the same mesh as that in presence of GNP in order to minimize variations caused by mesh. The boundary conditions on the GNP are removed and the inner volume of the GNP is integrated in the "Transport of Diluted Species" module. The maximum Electro-Motive Force (EMF) is computed with an insulating GNP, that is in absence of any depolarization of the solution. The maximum is taken as the difference of the potential of the solution between the two extremities of the GNP. The collection efficiency is defined as

$$CE = \frac{i_{UME}^{GNP} - i_{UME}^{bare}}{i_{GNP}}$$

where i_{UME}^{GNP}, i_{UME}^{bare} and i_{GNP} are the current simulated at the UME in presence of the GNP, the current simulated at the UME in absence of GNP, and the current simulated at the GNP, respectively.

The collection efficiency and the EMF as a function of the GNP-UME distance are shown in Figure S12, black and blue dots, respectively. As the GNP is further away in solution, the EMF drops. The concentration gradient fades away in solution and so is the collection efficiency. As the GNP gets close to the UME (within 500 nm, *d*/*a* less than 0.1), the collection rate tends to level off. We believe this trend is caused by the peculiar geometry of the "generator" shaped as a needle.

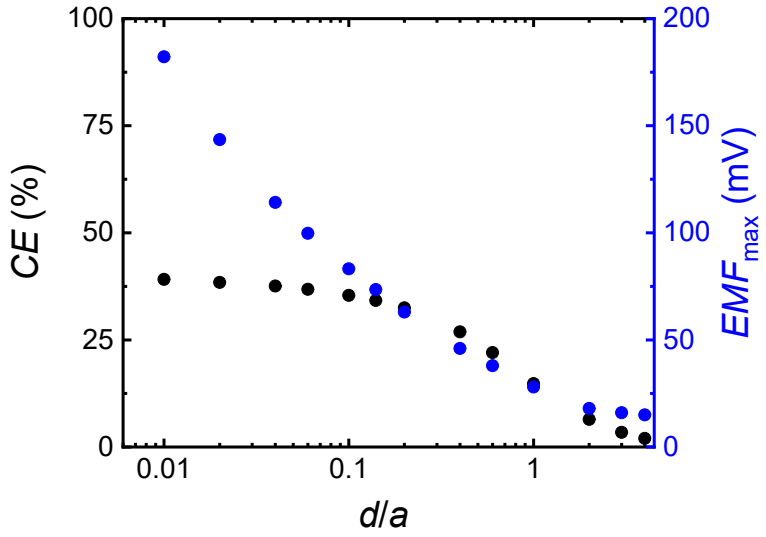

Figure S12. Collection efficiency simulated for a *L* = 5 µm tall and 1 µm large spheroidal GNP positioned at *d* above the surface of a = 5 µm radius UME

12. Estimation of the bipolar feedback detection scheme

Here we wish to address the question of the smallest detectable object. As long as the object is a good conductor (we do not consider discontinuous electronic states or Coulombic blockade) the chemical gradient in the diffusion layer will always drive a bipolar current at the surface of the object. The question is to determine whether or not this current can be detected. Our approach consists of detecting a small variation (0.1% to 1%) of current on top of a large signal. As we decrease the size of the object the bipolar feedback current will decrease (Figure 4D) ending up dwarfed by the noise of the large baseline current recorded at the UME in absence of the bipolar feedback.

Importantly, the magnitude of the bipolar feedback current scales linearly with the current at the UME (Figure 4A) and hence the size of the UME. It is thus expected that the size of the bipolar object can be scaled down as much as desired as long as the size of the UME is decreased in the same proportion. However, the signal-to-noise ratio of the setup and its bandwidth cannot stay constant as the current decreases, and eventually the increasing noise levels will hinder the detection of the bipolar feedback current setting a lower limit to the size of an object. According to Figure 5A an object having the same radius as the electrode and positioned at half a radius from the surface of the electrode produces 1% of the current variation. If the experimental setup allows the detection of a current variation of 0.1 pA, then the baseline current lies around 10 pA. Considering the steady-state oxidation of 3.8 mM FcDM, this size of the electrode is about 20 nm radius and thus an object of about the same size. This reasoning is confirmed by the numerical simulation of a spheroidal GNP of 20 and 4 nm width and length, respectively, positioned at 10 nm above the center of a 20 nm radius electrode. The simulated currents in absence and presence of the GNP are 16.57 pA and 16.64 pA, respectively. This difference corresponds to an increase of 0.4%, close to the 1% variation estimated above. Last but not least, we assume a bandwidth of 1 kHz to be sufficient for resolving the transient current feedback. For small objects, the velocities might be larger and require larger bandwidths. Increasing the concentration of redox mediator would produce larger currents and thus enable larger bandwidths.

13. The velocity of GNP approaching the UME

First, we assume that the angle between the GNP and the surface of the UME is constant during the approach and equal to (or very close) 90°. Recent observation of latex spheres, bacteria and GNPs approaching the surface of a UME revealed strong electro-osmotic flow directed from above the UME toward the center of the UME (when current is passing with low supporting electrolyte concentration).[5] Anisotropic objects like the GNPs preferentially orientate their long axis along this flow and thus arrive perpendicularly to the UME as described in our simulations. The ill-defined shape of the GNP is expected to introduce uncertainties in the absolute value of simulated currents. However, the relative variations of current are expected to be captured by the simulation. The calculation of the velocity of GNP approaching the UME is described step by step in Figure S13.

Figure S13 A shows the simulated bipolar feedback current as a function of the GNP-UME distance *d/a*. We used the red line as a simulated approach curve to deduce the distance *d* at every time during the chronoamperogram (the red line in Figure S13B). The distance *d* with respect to time is then plotted in Figure S13 C (black line). Then, we calculate the derivative of the black line to obtain the instantaneous velocity of the GNP along the direction normal to the surface (*V*z), as shown in the red line on the right axis. Finally, the velocity *V*z as a function of *d* (on a semi-log scale) is represented in Figure S13 D. Several µm from the surface the GNP seems to accelerate and then, at *d* = 0.5 µm decelerate from 10-15 µm/s to few µm/s.

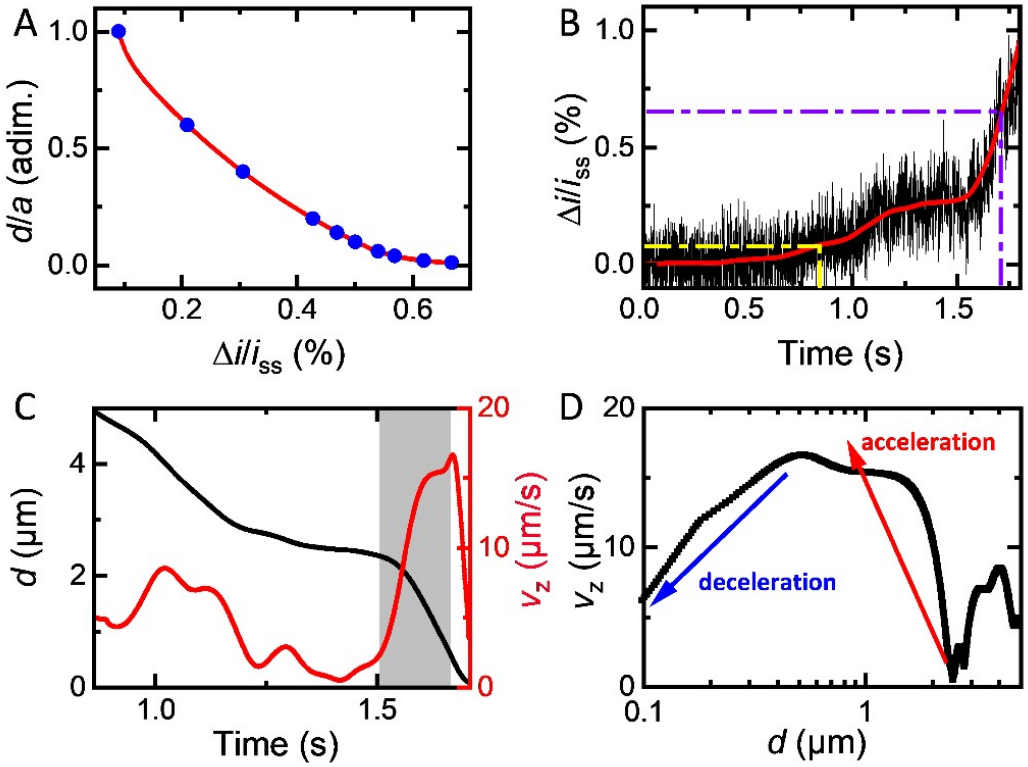

Figure S13. The procedure to calculate the velocity of GNP. (A) Simulated bipolar feedback current (blue dots) as a function of the GNP-UME distance *d/a*. (B) Normalized current trace by subtracting the baseline current (see Movie S2). The red line is the smoothed current trace and the truncated area (between yellow and violet dashed lines) corresponds to the ranges of 0.1% ~ 0.6% of bipolar feedback current in (A). (C) The black line shows the relation of *d* with respect to every time, and the red line is found by calculating the time-derivative of the black line. (D) The velocity of GNP plotted as a function of *d* on a semi-log scale.

14. Calculation of the Peclet number

The Peclet number, *Pe*, is defined as

$$Pe = \frac{dv}{D}$$

where *d* is the characteristic length of the system, *v* is the velocity and *D* is the diffusion coefficient. For a characteristic distance of 2 µm between the GNP and the surface of the electrode, the velocity is about 10 µm/s while at 0.1 µm we measure *v* = 1 µm/s.

For a prolate spheroidal object of long axis 2a and short axis 2b the diffusion coefficient along the direction of the long axis, $D_{\parallel}$, and along the short axis, $D_{\perp}$, are given by the expression[6-9]

$$D_{\parallel,\perp} = \frac{kT}{6\pi\eta b G_{\parallel,\perp}}$$

where *k*, *T* and η are the Boltzman constant, the temperature and the dynamic viscosity. The parameter *G* is defined as

$$G_{\parallel} = \frac{8}{3}\left[\frac{2p}{1-p^2} + \frac{2p^2-1}{(p^2-1)^{3/2}} ln\left(\frac{p+\sqrt{p^2-1}}{p-\sqrt{p^2-1}}\right)\right]^{-1}$$

$$G_{\perp} = \frac{8}{3}\left[\frac{p}{p^2-1} + \frac{2p^2-3}{(p^2-1)^{3/2}} ln\left(p+\sqrt{p^2-1}\right)\right]^{-1}$$

where $p=a/b$.

Since we consider the motion of the GNP mainly along the main axis (as shown in the video) we will use $D_{\parallel} = 10^{-8}$ cm²/s. We finally calculate *Pe* (@ 1 µm) = 10 and *Pe* (@ 0.1 µm) = 0.2.

15. Reference

1. Z. Deng, R. Elattar, F. Maroun and C. Renault, *Anal. Chem.*, 2018, **90**, 12923-12929.
2. R. Oldenbourg and M. Shribak, 2010, pp. 28.21-28.62.
3. N.-S. Cheng, *Ind. Eng. Chem. Res.*, 2008, **47**, 3285-3288.
4. Z. Deng, F. Maroun, J. E. Dick and C. Renault, *Electrochim. Acta*, 2020, **355**, 136805.
5. T. Moazzenzade, X. Yang, L. Walterbos, J. Huskens, C. Renault and S. G. Lemay, *J. Am. Chem. Soc.*, 2020, **142**, 17908-17912.
6. Z. Zheng and Y. Han, *J. Chem. Phys.*, 2010, **133**, 124509.
7. J. Happel and H. Brenner, *Low Reynolds number hydrodynamics: with special applications to particulate media*, Springer Science & Business Media, 2012.
8. F. Perrin, *J. Phys. Radium*, 1934, **5**, 497-511.
9. S. H. Koenig, *Biopolymers: Original Research on Biomolecules*, 1975, **14**, 2421-2423.